Control measures for thermal effects during placement of span-scale girder segments on continuous steel box girder bridges[*]

Jin-feng WANG[†], Jiang-tao ZHANG, Zhong-xuan YANG, Rong-qiao XU

Department of Civil Engineering, Zhejiang University, Hangzhou 310058, China

[†]E-mail: wangjinfeng@zju.edu.cn

Abstract: In this study, we examined the thermal effects throughout the process of the placement of span-scale girder segments on a 6×110-m continuous steel box girder in the Hong Kong-Zhuhai-Macao Bridge. Firstly, when a span-scale girder segment is temporarily stored in the open air, temperature gradients will significantly increase the maximum reaction force on temporary supports and cause local buckling at the bottom of the girder segment. Secondly, due to the temperature difference of the girder segments before and after girth-welding, some residual thermal deflections will appear on the girder segments because the boundary conditions of the structure are changed by the girth-welding. Thirdly, the thermal expansion and thermal bending of girder segments will cause movement and rotation of bearings, which must be considered in setting bearings. We propose control measures for these problems based on finite element method simulation with field-measured temperatures. The local buckling during open-air storage can be avoided by reasonably determining the appropriate positions of temporary supports using analysis of overall and local stresses. The residual thermal deflections can be overcome by performing girth-welding during a period when the vertical temperature difference of the girder is within 1 °C, such as after 22:00. Some formulas are proposed to determine the pre-set distances for bearings, in which the movement and rotation of the bearings due to dead loads and thermal loads are considered. Finally, the feasibility of these control measures in the placement of span-scale girder segments on a real continuous girder was verified: no local buckling was observed during open-air storage; the residual thermal deflections after girth-welding were controlled within 5 mm and the residual pre-set distances of bearings when the whole continuous girder reached its design state were controlled within 20 mm.

Key words: Steel box girder; Span-scale girder segments; Construction process; Thermal effects; Control measures

https://doi.org/10.1631/jzus.A1900310   **CLC number:** U445.467

1 Introduction

In a continuous steel box girder bridge, the girder is divided into many full-span segments, each of which is fabricated in factories, transported by ships, hoisted by a floating crane, and finally connected by girth-welding. This construction method is safe and efficient. However, to successfully position the segments and weld them together, the line shapes and stresses of the girder segments must be strictly controlled. Due to the low specific heat capacity and high thermal expansion coefficient of steel, the span-scale girder segments are affected by thermal stresses and deformations (Wang JF et al., 2016). Hence, it is imperative to analyze and control thermal effects during the placement of span-scale girder segments of a continuous steel box girder.

Temperature distribution in the girder is the basis of the study of thermal effects, and is determined by either code-specified temperature distribution scenarios or field-measured temperature results. Temperature distribution scenarios have been specified in design codes of many countries and regions, such as the EU, the USA, and China, to guide the design of their local bridges. However, cases arise where the actual temperature distribution in a girder becomes complex due to factors such as the intensity of solar radiation, shade temperature, humidity and flow speed of the air, and the structural style of the bridge. In such cases it is difficult for the code-specified temperature distribution scenarios to take account of these factors (Lucas et al., 2003; Zhou and Yi, 2013). Therefore, researchers are increasingly using field-measured temperatures to predict the temperature distribution in girders, and the results conform well with measured data (Tong et al., 2001, 2002; Ding et al., 2012; Miao and Shi, 2013; Wang GX et al., 2014; Kim et al., 2015; Wang JF et al., 2016). Considering a steel box girder under construction, its top plate is unpaved and directly exposed to sun radiation, while its web and bottom plate are primarily affected by diffuse solar radiation from the surrounding air. Therefore, there will be an obvious temperature difference along the depth of the girder in the daytime. Although transversal and longitudinal differences in temperature are usually far smaller than the vertical differences, there are still some special cases in which the transversal and longitudinal temperature differences cannot be ignored (Zhou and Yi, 2013; Kromanis et al., 2016). Therefore, the temperature distribution in a steel box girder should be carefully determined according to field-measured results.

Cases of non-uniformly distributed temperatures on a steel box girder are usually considered in relation to two types of thermal loads: uniform temperature changes and temperature gradients (Kim et al., 2009). Uniform temperature changes result in the thermal expansion of a steel box girder (Ding and Li, 2011; Lee et al., 2016), while temperature gradients, which are usually induced by the non-uniform radiation of sunlight, result in stresses and deformations on the girder (Moorty and Roeder, 1992; Malik et al., 2007; Xu et al., 2010; Wang JF et al., 2017). A temperature difference between the top and bottom surfaces of a

girder creates different levels of thermal expansion in the top and bottom plates. This causes "thermal bending" of the girder (Kowalski et al., 2018). Because of the great length of a span-scale girder segment, the thermal effects can be very significant (Li et al., 2009; Ding et al., 2012; Miao and Shi, 2013; Wang GX et al., 2014; Kim et al., 2015; Wang JF et al., 2016). For example, when there is a disparity between the assumed design installation temperature and the actual installation temperature of a bearing, thermal expansion and thermal bending will greatly affect the bottom plate length of the girder segment. This will cause movement and rotation of bearings under the girder segments, and so should be accurately predicted in the design stage (Kromanis et al., 2016). The assumed design installation temperature of a bearing is estimated by the field measurement of the shade temperature of air (Emerson, 1979). To ensure a bearing returns exactly to its undeformed shape after such a disparity occurs, the lower plate of the bearing should be longitudinally offset from its undeformed position by a certain pre-set distance. This is usually determined by simulation based on the distribution of temperature measured in the field. Similarly, based on those measurements, the thermal effects on the span-scale girder segments during other stages of the placement process should also be considered and studied by simulation.

The continuous steel box girders in the Hong Kong-Zhuhai-Macao Bridge (HZMB) were constructed by the span-scale girder segment placement technique. Unlike most other steel box girder bridges that used this technique, the span-scale girder segments of the HZMB are connected with both bolts and welds to prevent the fatigue cracking of the bridge deck. However, due to the limited adjustable distances of bolt holes, the requirement for accuracy in the construction of the HZMB is even higher than usual, and consequently the thermal effects during the whole placement process of the span-scale girder segments must be accurately predicted and well controlled. Using the placement of a 6×110-m continuous steel box girder in the HZMB as a case study, we investigated the thermal effects on the span-scale girder segments throughout the placement process, including during open-air storage, girth-welding, and the setting of bearings. We proposed some control measures to handle thermal effects during these construction

stages. The feasibility of these measures has been verified by their field application in the HZMB.

2 Project background

There are 24 pieces of 6×110-m continuous steel box girders in the non-navigable waters of the HZMB with a total length of 16 km. A 6×110-m continuous girder composed of six segments (Fig. 1) was selected to study the thermal effects during span-scale girder segment placement: the first segment was the longest (133 m) and the sixth segment the shortest (87 m). The other segments were each 110 m long. The continuous girder is a steel structure with a single box and double cells. It is 33.1 m wide and 4.5 m high (Fig. 2).

The HZMB is located in a subtropical zone with high temperatures all year round, and the placement of the sample continuous girder was performed in summer. The temperature distribution on the cross-section of the girder was measured by thermocouples located as shown in Fig. 2. The vertical temperature distribution of the field-measured temperatures during a summer day is shown in Fig. 3a. Compared to the vertical temperature difference, the transversal temperature difference was small and could be ignored (Wang JF et al., 2016). Because there were only

four thermocouples along the depth of the girder, Wang JF et al. (2016) studied the vertical temperature distribution in detail based on a simulation using a finite element analysis (FEA) model of the girder and the temperatures measured by the thermocouples. They found that the vertical temperature distribution could be simplified as a two-segment polyline along the depth of the girder (Fig. 3b). The temperature difference (T_1-T_2) between the top and bottom plates of the girder varied significantly with time. The average temperature difference in the daytime was 10 °C, and the maximum was 20 °C. At night, the average temperature difference fell to 1 °C between 22:00 and 7:00 the next day. Thus, when analyzing the thermal effects on the girder segments, the
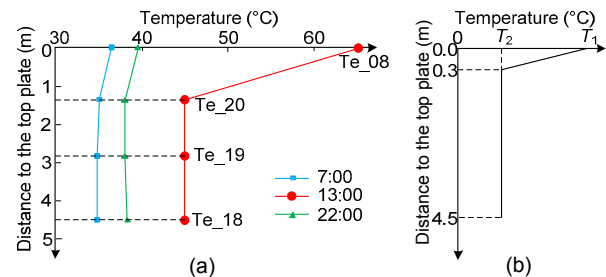

Fig. 3 Vertical temperature distribution of the cross-section: (a) results from field measurements on an extreme summer day; (b) a simplified scenario
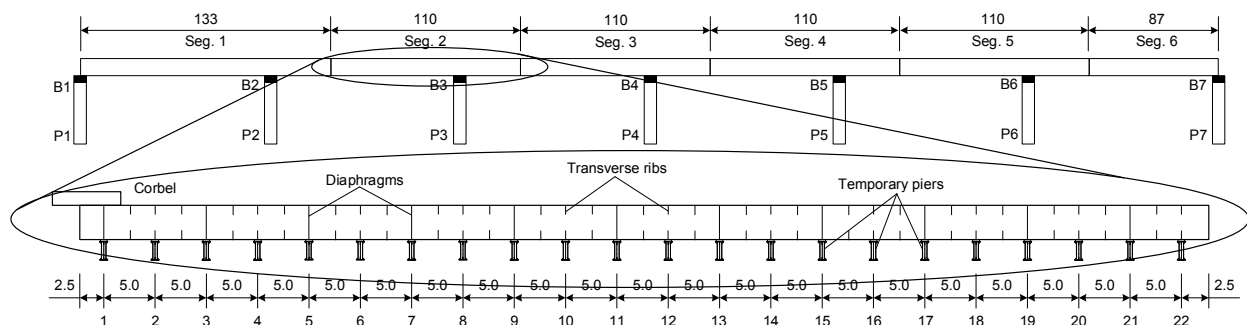

Fig. 1 Elevation of the girder segments (unit: m). The symbols 'Seg. *i*', 'B*i*', and 'P*i*' indicate the *i*th segment, the *i*th bearing, and the *i*th pier, respectively (*i*=1, 2, …, 7)
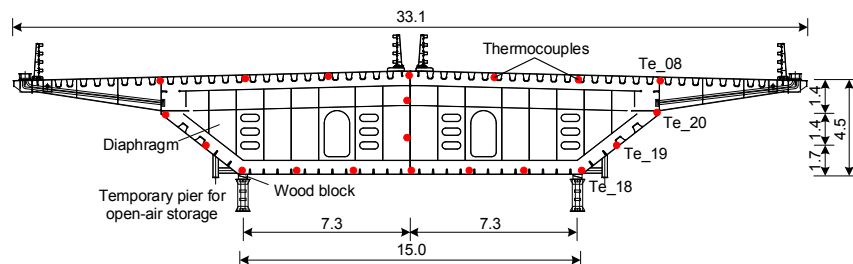

Fig. 2 Typical cross-section of a steel box girder (unit: m). The symbol 'Te' indicates temperature measurement point

temperature difference should be determined in relation to specific periods of the day.

Before placement starts, span-scale girder segments are temporarily placed in open-air yards waiting for shipment. During the waiting period, a certain number of piers should be arranged under the girder segment for temporary support. Considering a 110-m girder segment as an example, the longitudinal and transversal positions of the piers can be initially determined as shown in Figs. 1 and 2. In the initial plan (plan A), the piers are uniformly arranged along the length of the girder segment under the diaphragms or transverse ribs, at the stiffest places along the length of the girder. The area of contact of a pier with the girder segment is 400 mm×250 mm. However, the vertical temperature difference due to solar radiation will cause a thermal bending effect (Fig. 4a) (Kowalski et al., 2018). This effect results in a non-uniform distribution of reaction forces on piers along the length of the girder and significantly increases the maximum reaction force (Fig. 4b). Consequently, the buckling safety of the bottom plate should be checked according to the maximum observed temperature difference along the depth of the girder, i.e. where T_1=65 °C and T_2=45 °C. If the maximum reaction force of piers in plan A exceeds its permissible value, a new feasible plan (plan B) should be proposed instead.

After they are shipped to the construction site, the girder segments are hoisted and placed on temporary bearings by a floating crane. Fig. 5a indicates that, before girth-welding, two neighboring segments are connected by the corbel, as if they were "hinged" together (Fig. 5b). After girth-welding, the boundary conditions of the girder segments are changed from two hinged beams to a continuous beam (Figs. 5c and 5d). Consider a typical case where two neighboring segments are girth-welded under a certain temperature gradient in the daytime, and at night the temperature gradient disappears. Because the "hinge" connecting the two segments has been eliminated by the girth-welding, the thermal deflections created during the day do not simply recover. Therefore, the residual temperature-induced deformations and stresses on the segment should be carefully checked by simulation to guarantee the performance of the girder, and some appropriate control measures should be adopted.

After the girth-welding of two girder segments, the installation of permanent bearings begins on the earlier placed segment. The span-scale girder segment placement for a 6×110-m continuous steel box girder is divided into 16 procedures (Table 1). Pre-set distances for permanent bearings should be determined to ensure the aseismic performance of the bearings. The HZMB demands that the residual pre-set distance when the continuous girder reaches its design state should be less than 20 mm, which means the thermal effects of girder segments in determining the pre-set distances of permanent bearings must be accurately predicted.
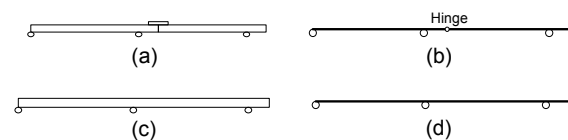

Fig. 5 Boundary condition change due to girth-welding of two girder segments: (a) sketch map before girth-welding; (b) boundary condition before girth-welding; (c) sketch map after girth-welding; (d) boundary condition after girth-welding
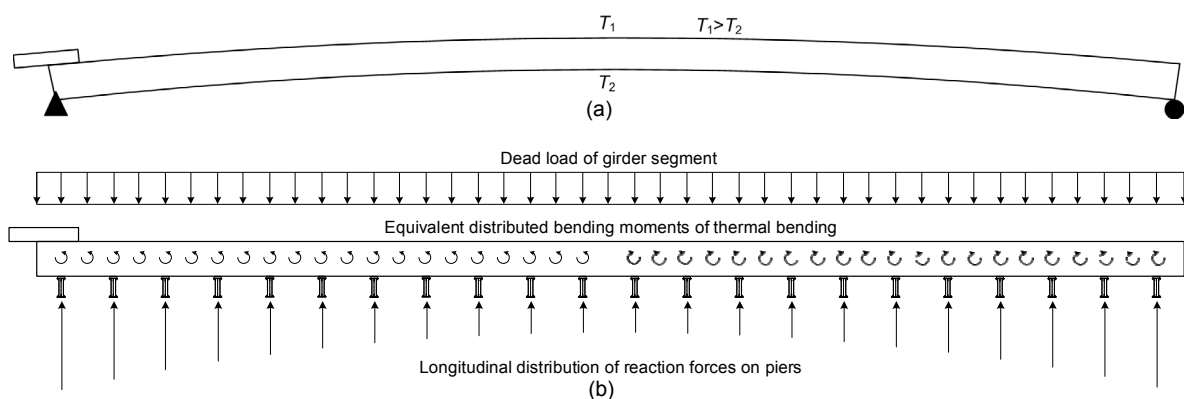

Fig. 4 Thermal effects on an open-air stored span-scale girder segment: (a) thermal bending; (b) distribution of reaction forces on piers considering thermal bending

Table 1 Span-scale girder segment placement procedures for a 6×110-m continuous girder

Order	Description	Illustration for boundary conditions of continuous girder
1	Hoisting Seg. 1	
2	Hoisting Seg. 2	
3	Girth-welding Seg. 2 and installing B1 & B2	
4	Hoisting Seg. 3	
5	Girth-welding Seg. 3 and installing B3	
6	Hoisting Seg. 4	
7	Girth-welding Seg. 4 and installing B4	
8	Transforming B4 into a fixed bearing	
9	Transforming B2 into a sliding bearing	
10	Hoisting Seg. 5	
11	Girth-welding Seg. 5 and installing B5	
12	Hoisting Seg. 6	
13	Girth-welding Seg. 6 and installing B6	
14	Installing B7	
15	Applying secondary dead loads	
16	Design state of the girder	

△ Temporary sliding bearing
○ Temporary clamped bearing
▲ Permanent sliding bearing
● Permanent clamped bearing
⊓ Corbel

3   Thermal effects on an open-air stored span-scale girder segment

To check the buckling safety of the bottom plate on a span-scale girder segment during open-air storage, an FEA model of the 110-m girder segment was created using the software ABAQUS with shell elements S8R, and used to determine the permissible reaction force for a single pier (Fig. 6). The reaction force for each pier was considered to consist of uniformly distributed loads in the contact regions (400 mm× 250 mm) under the diaphragms and transverse ribs. According to the Chinese steel structure design code GB50017 (MOHURD, 2003), the permissible stress of the girder is 310 MPa (Q345 steel). When the reaction force loaded in the model was increased to 783.5 kN, the maximum stress under the diaphragms reached 310 MPa, but was still within the permissible range under the transverse ribs. Hence, the permissible reaction force for a single pier is 783.5 kN.

Considering the symmetry of the transversal distribution of the supporting piers, the reaction forces are equal along the width of the girder segment, but the maximum reaction force on the piers should be checked along the length of the girder. To calculate the actual maximum reaction forces (Fig. 7) for piers
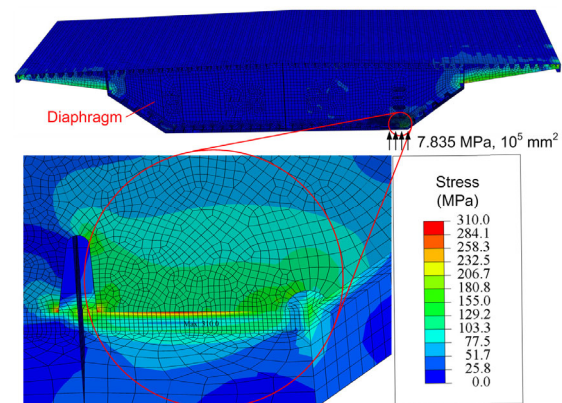
Fig. 6 Determining the permissible reaction force for a single pier

Fig. 7 FEA model of a 110-m girder segment (plan A)

in plan A, another model of the 110-m segment was established using the FEA software Midas Civil with spatial beam elements.

The longitudinal distribution of the reaction forces for a single pier in plan A is shown in Fig. 8. When the temperature gradient is ignored, the maximum reaction force for a single pier is 664 kN at the end of the girder segment on the corbel side. That is less than the permissible value 783.5 kN, which

indicates that plan A is safe when the temperature gradient is ignored. However, when the temperature gradient is considered, the maximum reaction force for a single pier builds up to 1507.5 kN, which far exceeds the permissible value. These results indicate that the temperature gradient will cause local buckling on the bottom plate of the girder segments in plan A, and thus a new feasible plan for arrangement of the supporting piers should be proposed.

The new plan can be determined based on plan A by setting additional piers along the length of the girder segment to reduce the maximum reaction force on a single pier until the value is less than 783.5 kN. Compared with plan A, the area of the contact region between a single pier and the girder segment is unchanged, and the new added piers are also set under the transverse ribs of the girder segment. In particular, considering the greatest reaction forces are located at the two ends along the length of the girder segment, one more pier can be added in these positions under the center of the bottom plate along its width to further reduce the maximum reaction force. According to these principles, plan B is proposed (Fig. 9). The longitudinal row number of the arranged piers is increased from 22 to 33, as some additional rows of piers are added under the transverse ribs every 10 m along the length of the girder segment. The transversal numbers of arranged piers in each of the 1st, 2nd, 32nd, and 33rd rows are increased from 2 to 3. The longitudinal distribution of the reaction forces acting on a single pier in plan B was compared with that of plan A (Fig. 10). Considering the thermal effects, the

maximum reaction force for a single pier still appears at the end of the girder segment on the corbel side, but is reduced to 711.3 kN in plan B, which is within the permissible range. Consequently, plan B is proved to be theoretically safe even in extremely hot weather conditions. Furthermore, plan B was applied in the field to the open-air storage of the span-scale girder segments of the HZMB. No local buckling deformations were observed on the open-air stored girder segments, therefore the safety of plan B was proved in practice.

4 Thermal effects during the boundary condition change due to girth-welding

To observe thermal effects during the boundary condition change due to girth-welding, a FEA model
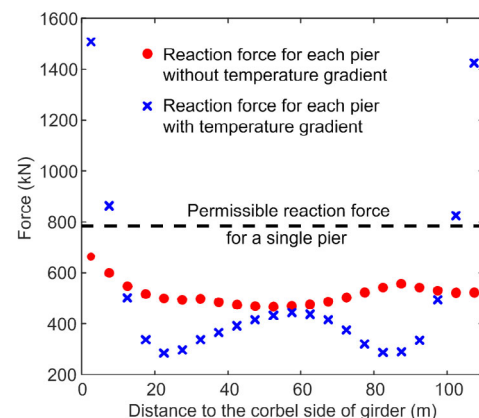

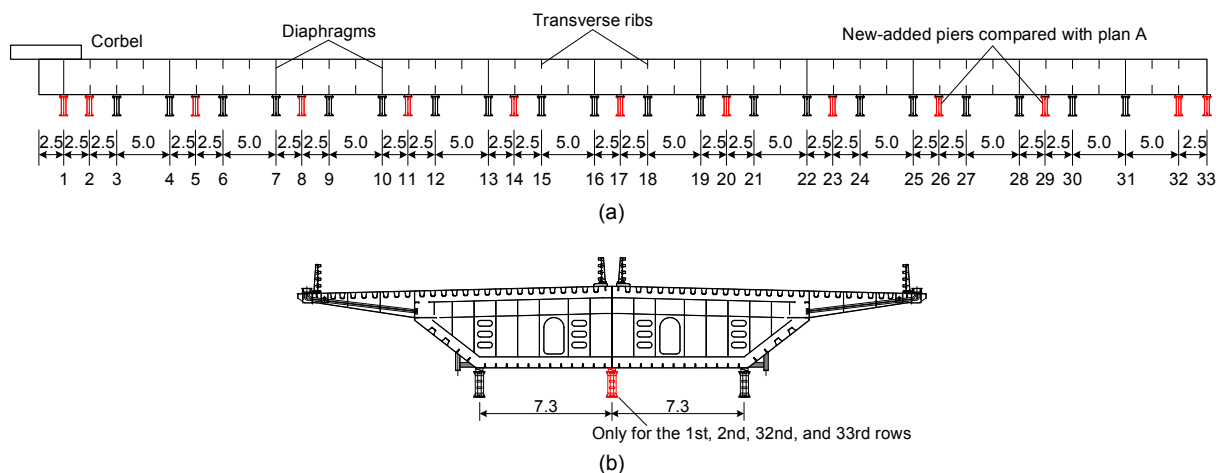**Fig. 8 Longitudinal distribution of reaction forces for each pier (plan A)**

Fig. 9 Plan B for the arrangement of supporting piers: (a) longitudinal; (b) transversal (unit: m)

for the first two span-scale girder segments (segments 1 and 2) was established in the FEA software Midas Civil with spatial beam elements (Fig. 11). Considering the most general situation of daytime in summer, 40 °C and 30 °C were respectively adopted as T_1 and T_2 of the temperature scenario along the depth of the girder in the model.

Fig. 12 depicts the longitudinal distribution of thermal deflections when two neighboring girder segments are girth-welded under a vertical temperature difference of 10 °C and the temperature difference disappears when the weld is done. Because the temperatures of the top plate are much higher than those of the bottom plate, the deflections between the two bearings B1 and B2 are upward due to thermal bending. Since point B is a free end of segment 1, the deflections from point B_2 to point B are downward. Segment 2 is "hinged" on segment 1 at point B (Fig. 5b). When the girder segment between points B and B_3 moves upward due to thermal bending, a sharp change appears in the deflection curve of the two segments at point B. After the "hinge" at point B is eliminated by girth-welding, the thermal deflections cannot recover with the disappearance of thermal loads. The maximum residual thermal deflection, −41 mm, is downward at the girth-welded joint (point B). The maximum upward residual thermal deflections

of the two segments, 30 mm and 3 mm, appear at the positions of 65 m and 192.5 m from bearing B1 (points A and C), respectively.

Selecting points A, B, and C as three typical points, their residual thermal deflections after girth-welding with different vertical temperature differences on the girder were studied (Fig. 13). The residual thermal deflections of the three points approximately exhibit a linear relationship with the vertical temperature difference in girth-welding. The residual thermal deflections are not obvious when the
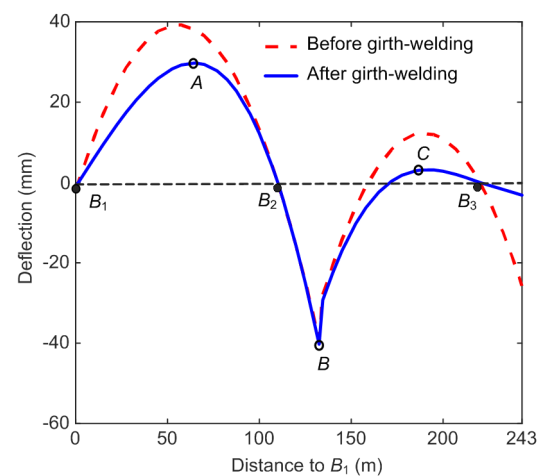

Fig. 12 Thermal deflections of two girder segments when girth-welded under a vertical temperature difference of 10 °C and thermal loads disappear after completion of the weld
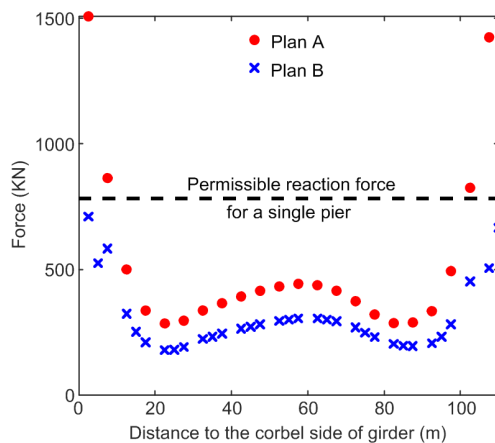

Fig. 10 Longitudinal distribution of reaction forces on each pier in the two plans
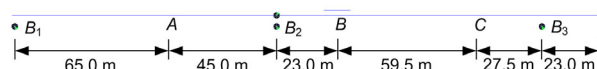

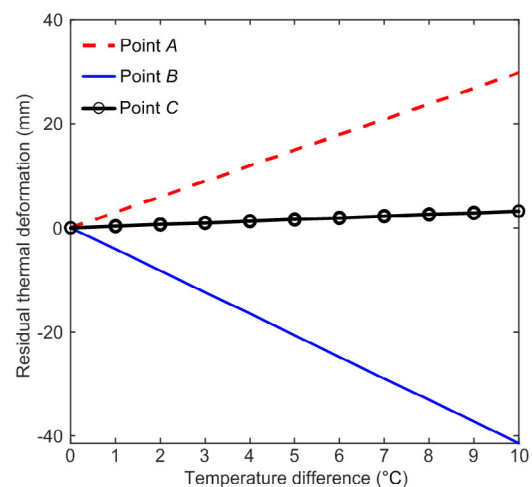**Fig. 11 FEA model of segments 1 and 2**

Fig. 13 Residual thermal deflections of three typical points after girth-welding with different vertical temperature differences on the girder

vertical temperature difference is small. Thus, the requirement of the HZMB can be met by controlling the vertical temperature difference within a 1 °C range during girth-welding, which can be realized at night from 22:00 to 7:00 the next day. Therefore, this period was chosen to perform the girth-welding of the real girder segments in the HZMB, and the thermal deflections were observed to have been effectively controlled in the field application.

5 Thermal effects in pre-setting distances for sliding bearings

Based on beam theory, though the neutral layer of the girder segment will not be lengthened or shortened by a dead load, the upper plates of the sliding bearings, which are fixed on the bottom plate of the girder segments, will be moved longitudinally with the progress of girder placement. When segment 2 is hung on segment 1 through its corbel, the dead load of segment 2 will cause a movement δ^{g} (the superscript "g" indicates "gravity") and a rotation $\theta_2-\theta_1$ of the upper bearing plate of the sliding bearing B1 (Fig. 14). Thermal expansion and thermal bending due to a uniform temperature change and a temperature gradient, respectively, will cause similar effects. Thus, to ensure a sliding bearing returns exactly to its undeformed shape when the whole continuous girder reaches its design state, a pre-set distance Δ^{p} should be determined for the bearing (Fig. 15). This requires accurate prediction of the effects of dead load and thermal loads on the girder after installation of the bearings. Another distance called the overall offset, Δ^{o}, should also be pre-set for positioning the girder segment, since the upper bearing plate is moved by dead loads and thermal loads before installation of the bearing.

The pre-set distance is determined by the variation in the length of the bottom plate of the girder segment between the centerlines of the considered sliding bearing and its nearest fixed bearing, which is affected by dead loads and thermal loads. Taking the forward direction of construction as the positive direction of displacement, if the placement for a steel continuous box girder takes n procedures to reach its design state, and its jth bearing is installed in the mth
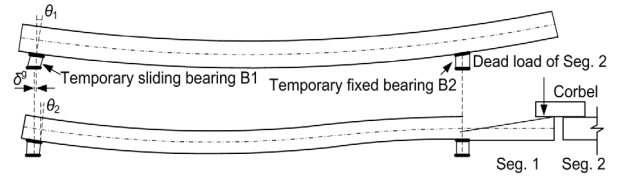

Fig. 14 Movement and rotation of a sliding bearing of segment 1 under the dead load of segment 2
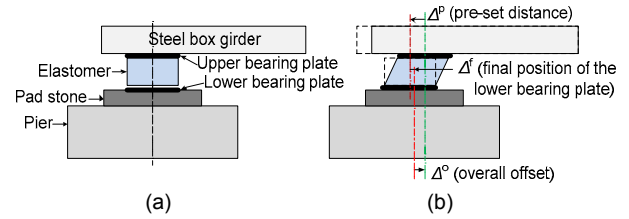

Fig. 15 Pre-setting distances for a sliding bearing: (a) design state of bearing; (b) pre-setting distance for bearing

procedure, the pre-set distance for the bearing, Δ_j^{p}, can be expressed as

$$\Delta_j^{p} = -c_{nj}\alpha L_{nj}(T^{d} - T_j^{a}) - \sum_{i=m+1}^{n} c_{ij}\boldsymbol{l}_{ij}^{\mathrm{T}}\frac{\boldsymbol{\sigma}_{ij}}{E}, \qquad (1)$$

where c_{ij} is the state parameters of the jth bearing in the ith procedure: $c_{ij}=0$ for fixed bearings, $c_{ij}=1$ for sliding bearings in the forward direction of construction, and $c_{ij}=-1$ for sliding bearings in the backward direction of construction; α is the thermal expansion coefficient of steel; L_{nj} is the cantilever length of the bottom girder plate from the jth bearing to the fixed bearing in the design state of the girder; T^{d} is the design assumed installation temperature of the considered bearing; T_j^{a} is the actual installation temperature of the jth bearing; $\boldsymbol{l}_{ij} = [l_{ij}^{1} \; \cdots \; l_{ij}^{k} \; \cdots \; l_{ij}^{s_{ij}}]^{\mathrm{T}}$, where l_{ij}^{k} is the length of the kth element on the bottom plate of girder from the jth bearing to its nearest fixed bearing in the FEA model of the ith procedure, and s_{ij} is the total number of beam elements on the bottom plate from the jth bearing to its nearest fixed bearing in the FEA model of the ith procedure; $\boldsymbol{\sigma}_{ij} = [\sigma_{ij}^{1} \; \cdots \; \sigma_{ij}^{k} \; \cdots \; \sigma_{ij}^{s_{ij}}]^{\mathrm{T}}$, where σ_{ij}^{k} is the variation in the stress of the bottom edge of the kth element on the bottom girder plate from the jth bearing to its

nearest fixed bearing in the FEA model of the *i*th procedure due to the dead load and temperature gradient; E is the elastic modulus of steel.

Similarly, the "overall offset" for positioning the girder segments and the upper plate of the *j*th bearing, Δ_j^o, can be expressed as

$$\Delta_j^o = c_{nj}\alpha L_{nj}(T_j^a - T^d) + \sum_{i=1}^{m} c_{ij}\boldsymbol{l}_{ij}^{\mathrm{T}}\frac{\boldsymbol{\sigma}_{ij}}{E}. \tag{2}$$

The final position for the lower plate of the *j*th bearing, Δ_j^f, is expressed as

$$\Delta_j^f = \Delta_j^p + \Delta_j^o. \tag{3}$$

As shown in Table 1, the parameters in Eqs. (1)–(3) for the erection of the considered continuous girder can be determined as follows:

$$\boldsymbol{C} = \begin{bmatrix} -1 & 0 & 0 & 0 & 0 & 0 & 0 \\ -1 & 0 & 1 & 0 & 0 & 0 & 0 \\ -1 & 0 & 1 & 0 & 0 & 0 & 0 \\ -1 & 0 & 1 & 1 & 0 & 0 & 0 \\ -1 & 0 & 1 & 1 & 0 & 0 & 0 \\ -1 & 0 & 1 & 1 & 1 & 0 & 0 \\ -1 & 0 & 1 & 1 & 1 & 0 & 0 \\ -1 & 0 & 0 & 0 & 1 & 0 & 0 \\ -1 & -1 & -1 & 0 & 1 & 0 & 0 \\ -1 & -1 & -1 & 0 & 1 & 1 & 0 \\ -1 & -1 & -1 & 0 & 1 & 1 & 0 \\ -1 & -1 & -1 & 0 & 1 & 1 & 1 \\ -1 & -1 & -1 & 0 & 1 & 1 & 1 \\ -1 & -1 & -1 & 0 & 1 & 1 & 1 \\ -1 & -1 & -1 & 0 & 1 & 1 & 1 \\ -1 & -1 & -1 & 0 & 1 & 1 & 1 \end{bmatrix}, \tag{4}$$

$$\boldsymbol{L} = \begin{bmatrix} 328.5 \\ 220 \\ 110 \\ 0 \\ 110 \\ 220 \\ 328.5 \end{bmatrix}, \tag{5}$$

where $\boldsymbol{C}=\{c_{ij}\}_{16\times7}$ is the state parameter matrix of the bearings; $\boldsymbol{L}=\{L_{nj}\}_{7\times1}$ is the cantilever length vector of the bearings; $\alpha=1.2\times10^{-5}$ °C^{-1} for steel; $T^d=$ 22.7 °C for all springs.

According to the field-measured temperatures, on a spring, summer, autumn, or winter night, T_j^a should be 12 °C, 27 °C, 24 °C, and 7 °C, while the temperature difference between the top and bottom plates of the girder should be 1 °C, 2 °C, 2 °C, and 0 °C, respectively. Taking the bearings of the sample continuous girder as an example, if they are installed at night in different seasons, the overall offset, pre-set distance, and final position of each bearing should be set as shown in Tables 2 and 3 (p.265). The results show that the pre-set distances vary significantly with seasonal temperature changes.

However, the bearings are usually installed in the daytime. Therefore, if we consider the bearings of the same continuous girder are installed at noon in summer, then the pre-set distance, overall offset, and final position for each bearing are determined according to the measured temperatures shown in Table 4 (p.266) (T_1=40 °C, T_2=30 °C). Finally, the bearings of the real continuous girder were set and installed in summer at noon based on these results. Taking bearing B1 as an example, the field-measured residual pre-set distance when the girder reached its design state was 12 mm (Fig. 16). The results for other bearings were all less than the maximum permissible distance of 20 mm (Table 5) (p.266). This indicates that the thermal effects before and after installation of the sliding bearings of the HZMB were successfully predicted and well controlled by pre-setting distances based on the field-measured temperatures.
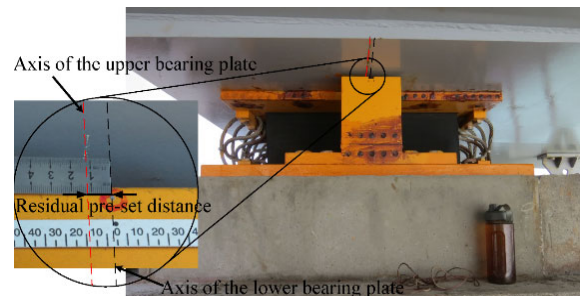

Fig. 16 Field-measured residual pre-set distance for bearing B1

Table 2 Pre-set distances and final positions for bearings at night in spring and summer
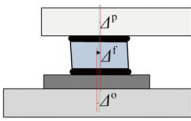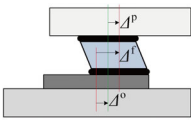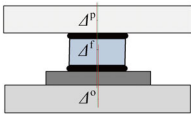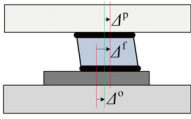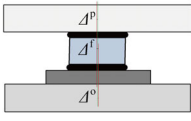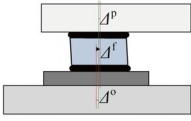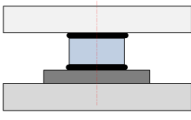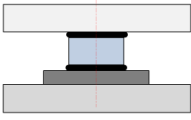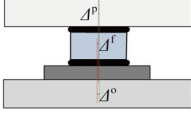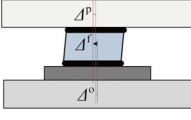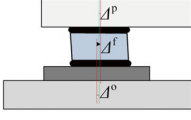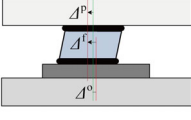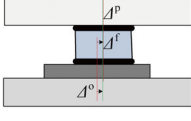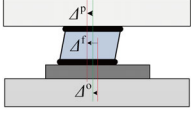
Bearing	Spring				Summer			
	Δ^{o} (mm)	Δ^{p} (mm)	Δ^{f} (mm)	Illustration	Δ^{o} (mm)	Δ^{p} (mm)	Δ^{f} (mm)	Illustration
B1	64.20	54.65	118.85		5.08	−4.68	0.40	
B2	28.25	30.54	58.79		−11.35	−9.23	−20.58	
B3	11.59	13.28	24.87		−8.24	−6.61	−14.85	
B4	0.00	0.00	0.00		0.00	0.00	0.00	
B5	−4.08	−20.29	−24.37		15.78	−0.58	15.20	
B6	−11.65	−28.17	−39.81		28.00	11.28	39.28	
B7	−2.29	−46.32	−48.61		56.85	12.62	69.47	

6 Conclusions

In this study, we investigated the thermal effects on the placement of span-scale girder segments of a continuous steel box girder during open-air storage, girth-welding, and setting bearings. Based on the results, some control measures were proposed. In the open-air storage of a span-scale girder segment, the temperature gradient along the depth of the girder segment will greatly increase the maximum reaction force on temporary piers and cause local buckling of the bottom plate under the girder segment. Based on a simulation with field-measured temperatures, an improved arrangement plan involving additional support piers was proposed to reduce the maximum reaction force. In the field application of the improved arrangement plan during open-air storage, no local buckling was observed. During girth-welding of two girder segments, the temperature difference before and after girth-welding caused some residual thermal deflections on the girder due to a change in the boundary conditions of the structure. The vertical temperature difference in girth-welding should be

Table 3 Pre-set distances and final positions for bearings at night in autumn and winter

Bearing	Autumn				Winter			
	Δ^o (mm)	Δ^p (mm)	Δ^f (mm)	Illustration	Δ^o (mm)	Δ^p (mm)	Δ^f (mm)	Illustration
B1	16.91	7.15	24.05		83.91	74.55	158.46	
B2	−3.43	−1.31	−4.74		41.45	43.91	85.36	
B3	−4.28	−2.65	−6.93		18.23	19.97	38.19	
B4	0.00	0.00	0.00		0.00	0.00	0.00	
B5	11.82	−4.54	7.28		−10.73	−26.80	−37.53	
B6	20.08	3.36	23.44		−24.89	−41.21	−66.10	
B7	45.02	0.79	45.82		−22.02	−65.84	−87.85	

controlled within 1 °C to reduce the maximum residual thermal deflection. This can be realized by performing girth-welding in a specific period at night, such as after 22:00. In the field application of this control measure during girth-welding, the residual thermal deflections were controlled within 5 mm.

The pre-set distance of bearings should include the variation in the length of the bottom girder plate due to three factors: dead load, temperature gradient, and uniform temperature change. Here, we proposed formulas for the pre-set distance, overall offset, and final position for sliding bearings, in which the parameters were determined based on the field-measured temperature data. In the field application of these formulas during bearing installation, the residual pre-set distances for bearings were controlled within 20 mm after the structural temperature was changed to their assumed design installation temperature. The proposed control measures have successfully controlled the thermal effects in the span-scale girder segment placement of a continuous steel box girder in the HZMB, and thus they are also applicable to other continuous steel box girder bridges.

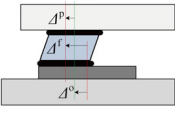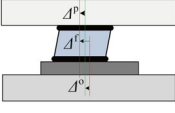**Table 4 Pre-set distances and final positions for the bearings in summer at noon**
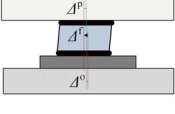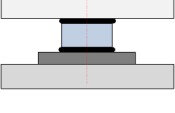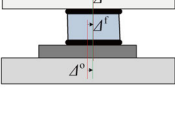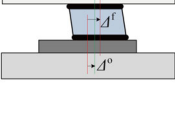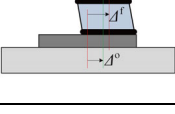
Bearing	Δ^{o} (mm)	Δ^{p} (mm)	Δ^{f} (mm)	Illustration
B1	−92.52	−73.81	−166.30	
B2	−32.47	−37.40	−69.87	
B3	−11.24	−14.72	−25.96	
B4	0.00	0.00	0.00	
B5	36.22	4.09	40.31	
B6	65.59	32.95	98.54	
B7	128.20	40.59	168.80	

Table 5 Residual pre-set distances for the bearings installed in summer at noon

Bearing	Residual pre-set distance (mm)
B1	−12.0
B2	−4.8
B3	−3.7
B4	4.1
B5	3.1
B6	4.3
B7	7.4

Contributors

Jin-feng WANG conceptualized the research. Jiang-tao ZHANG processed the corresponding data and wrote the first draft of the manuscript. Jin-feng WANG and Rong-qiao XU helped to organize the manuscript. Jin-feng WANG and Zhong-xuan YANG revised and edited the final version.

Conflict of interest

Jin-feng WANG, Jiang-tao ZHANG, Zhong-xuan YANG, and Rong-qiao XU declare that they have no conflict of interest.

References

Ding YL, Li AQ, 2011. Temperature-induced variations of measured modal frequencies of steel box girder for a long-span suspension bridge. *International Journal of Steel Structures*, 11(2):145-155.
https://doi.org/10.1007/s13296-011-2004-4

Ding YL, Zhou GD, Li AQ, et al., 2012. Thermal field characteristic analysis of steel box girder based on long-term measurement data. *International Journal of Steel Structures*, 12(2):219-232.
https://doi.org/10.1007/s13296-012-2006-x

Emerson M, 1979. Bridge Temperatures for Setting Bearings and Expansion Joints. Technical Report No. SR479, Transport and Road Research Laboratory, Wokingham, UK.

Kim SH, Cho KI, Won JH, et al., 2009. A study on thermal behaviour of curved steel box girder bridges considering solar radiation. *Archives of Civil and Mechanical Engineering*, 9(3):59-76.
https://doi.org/10.1016/S1644-9665(12)60218-0

Kim SH, Park SJ, Wu JX, et al., 2015. Temperature variation in steel box girders of cable-stayed bridges during construction. *Journal of Constructional Steel Research*, 112(1):80-92.
https://doi.org/10.1016/j.jcsr.2015.04.016

Kowalski R, Głowacki M, Wróblewska J, 2018. Thermal bowing of reinforced concrete elements exposed to non-uniform heating. *Archives of Civil Engineering*, 64(4):247-264.
https://doi.org/10.2478/ace-2018-0055

Kromanis R, Kripakaran P, Harvey B, 2016. Long-term structural health monitoring of the Cleddau Bridge: evaluation of quasi-static temperature effects on bearing movements. *Structure and Infrastructure Engineering*, 12(10):1342-1355.
https://doi.org/10.1080/15732479.2015.1117113

Lee JH, Jeong YS, Kim WS, 2016. Buckling behavior of steel girder in integral abutment bridges under thermal loadings in summer season during deck replacement. *International Journal of Steel Structures*, 16(4):1071-1082.
https://doi.org/10.1007/s13296-016-0023-x

Li CX, Yang N, Zhang YP, et al., 2009. The sunlight thermal gradient of the steel box girder and the deformation of the last girder in incremental launching construction of

Hangzhou Jiangdong Bridge. *Journal of Transport Science and Engineering*, 25(1):39-44 (in Chinese).
https://doi.org/10.3969/j.issn.1674-599X.2009.01.008

Lucas JM, Berred A, Louis C, 2003. Thermal actions on a steel box girder bridge. *Proceedings of the Institution of Civil Engineers–Structures and Buildings*, 156(2):175-182.
https://doi.org/10.1680/stbu.156.2.175.37868

Malik P, Kadoli R, Ganesan N, 2007. Effect of boundary conditions and convection on thermally induced motion of beams subjected to internal heating. *Journal of Zhejiang University-SCIENCE A*, 8(7):1044-1052.
https://doi.org/10.1631/jzus.2007.A1044

Miao CQ, Shi CH, 2013. Temperature gradient and its effect on flat steel box girder of long-span suspension bridge. *Science China Technological Sciences*, 56(8):1929-1939.
https://doi.org/10.1007/s11431-013-5280-8

MOHURD (Ministry of Housing and Urban-Rural Development of the People's Republic of China), 2003. Code for Design of Steel Structures, GB50017-2003. National Standards of the People's Republic of China, Beijing, China (in Chinese).

Moorty S, Roeder CW, 1992. Temperature-dependent bridge movements. *Journal of Structural Engineering*, 118(4): 1090-1105.
https://doi.org/10.1061/(asce)0733-9445(1992)118:4(1090)

Tong M, Tham LG, Au FTK, et al., 2001. Numerical modelling for temperature distribution in steel bridges. *Computers & Structures*, 79(6):583-593.
https://doi.org/10.1016/S0045-7949(00)00161-9

Tong M, Tham LG, Au FTK, 2002. Extreme thermal loading on steel bridges in tropical region. *Journal of Bridge Engineering*, 7(6):357-366.
https://doi.org/10.1061/(asce)1084-0702(2002)7:6(357)

Wang GX, Ding YL, Wang XJ, et al., 2014. Long-term temperature monitoring and statistical analysis on the flat steel-box girder of Sutong Bridge. *Journal of Highway and Transportation Research and Development (English Edition)*, 8(4):63-68.
https://doi.org/10.1061/JHTRCQ.0000412

Wang JF, Zhang L, Xiang HW, et al., 2016. Temperature effect during construction of non-navigable bridge of Hong Kong-Zhuhai-Macao Bridge over deep water area. *China Journal of Highway and Transport*, 29(12):70-77 (in Chinese).
https://doi.org/10.19721/j.cnki.1001-7372.2016.12.009

Wang JF, Xu ZY, Fan XL, et al., 2017. Thermal effects on curved steel box girder bridges and their countermeasures. *Journal of Performance of Constructed Facilities*, 31(2): 04016091.
https://doi.org/10.1061/(asce)cf.1943-5509.0000952

Xu YL, Chen B, Ng CL, et al., 2010. Monitoring temperature effect on a long suspension bridge. *Structural Control and Health Monitoring*, 17(6):632-653.
https://doi.org/10.1002/stc.340

Zhou GD, Yi TH, 2013. Thermal load in large-scale bridges: a state-of-the-art review. *International Journal of Distributed Sensor Networks*, 161(4):85-93.
https://doi.org/10.1155/2013/217983

<u>中文概要</u>

题　目：连续钢箱梁桥整孔安装施工全过程的温度效应控制措施

目　的：采用整孔安装的连续钢箱梁对施工精度要求极高，而其在露天存放、环缝焊接和设置支座预偏量等环节会不可避免地受温度变化的影响而产生应力和位移，因此应引起特别关注。首先，置于露天场地存放的钢箱梁节段各处受到的日光照射不均匀，由此产生的截面竖向温度梯度会使梁底临时支墩的反力分布出现巨大变化，从而影响箱梁节段的局部受力安全；其次，因为环缝焊接会使相邻梁段结构体系从简支梁变成连续梁，所以在焊接过程中若箱梁顶底板因存在温差而引起了变形，则该变形在焊接后不会随着温差的减小而逐步消除；最后，连接在箱梁底板上的滑动支座顶板在支座安装完成后仍会受温度影响而发生位移。为了使永久支座在施工完毕后的顶底板中心线对齐，在安装支座时需要考虑这些位移并对支座进行预偏。

创新点：1. 发现温度梯度会导致露天存放的大节段钢箱梁下局部支墩反力的大幅度增加；2. 发现在环缝焊接时箱梁截面温度梯度导致的位移不会在焊接后随着温度梯度的消失而减小，这是因为箱梁的边界条件发生了变化；3. 提出了考虑温度效应的支座预偏量公式；4. 针对这些温度效应提出了应对策略。

方　法：1. 根据钢箱梁截面的实测温度数据（图3），建立连续钢箱梁施工全过程的有限元分析模型；2. 通过有限元模型的计算结果，对钢箱梁在露天存放、环缝焊接及设置支座预偏量时的温度效应展开分析研究，并给出相应的解决方案；3. 将解决方案应用于实际桥梁施工中，以验证所提方法的可行性和有效性。

结　论：1. 钢箱梁在露天存放、环缝焊接及设置支座预偏量时的温度效应会严重影响钢箱梁的整孔安装施工，因此必须得到有效控制；2. 利用钢箱梁截面的实测温度数据建立钢箱梁施工全过程的有限元模型，可对施工过程中的温度效应进行预测并据此提出控制措施；3. 钢箱梁的成功施工验证了本文所提出的温度效应控制措施的有效性，这对同类工程的施工具有借鉴意义和参考价值。

关键词：钢箱梁；整孔安装；施工过程；温度效应；控制措施